Published in final edited form as:
Science. 2012 August 3; 337(6094): 591–595. doi:10.1126/science.1218716.

OPENING AND CLOSING OF THE BACTERIAL RNA POLYMERASE CLAMP:

Single-molecule fluorescence experiments define RNA polymerase clamp conformation in transcription initiation and elongation

Anirban Chakraborty[1], **Dongye Wang**[1], **Yon W. Ebright**[1], **You Korlann**[2], **Ekaterine Kortkhonjia**[1,2], **Saikat Chowdhury**[3], **Sivaramesh Wigneshweraraj**[4], **Herbert Irschik**[5], **Rolf Jansen**[5], **B. Tracy Nixon**[3], **Jennifer Knight**[6], **Shimon Weiss**[2], and **Richard H. Ebright**[1,*]

[1]Howard Hughes Medical Institute, Waksman Institute, and Department of Chemistry and Chemical Biology, Rutgers University, Piscataway NJ 08854, USA

[2]Department of Chemistry and Biochemistry, UCLA, Los Angeles CA 90095, USA

[3]Department of Biochemistry, Pennsylvania State University, State College PA 16802, USA

[4]Centre for Molecular Microbiology and Infection, Imperial College London, SW7 2AZ, UK

[5]Helmholtz Centre for Infection Research, 38124 Braunschweig, Germany

[6]Department of Chemistry, University of Michigan, Ann Arbor MI 48109, USA

Abstract

Using single-molecule fluorescence resonance energy transfer, we have defined bacterial RNA polymerase (RNAP) clamp formation at each step in transcription initiation and elongation. We find that the clamp predominantly is open in free RNAP and early intermediates in transcription initiation, but closes upon formation of a catalytically competent transcription initiation complex and remains closed during initial transcription and transcription elongation. We show that four RNAP inhibitors interfere with clamp opening. We propose that clamp opening allows DNA to be loaded into and unwound in the RNAP active-center cleft, that DNA loading and unwinding trigger clamp closure, and that clamp closure accounts for the high stability of initiation complexes and the high stability and processivity of elongation complexes.

RNA polymerase (RNAP) has a structure that resembles a crab claw, with two "pincers" surrounding a cleft that contains the RNAP active-center and serves as the binding site for DNA (Fig. 1A; 1-4). RNAP is a multi-subunit protein. The largest subunit (β' in bacterial RNAP) forms one pincer, termed the "clamp". The second-largest subunit (β in bacterial RNAP) forms the other pincer. Crystal structures of RNAP in different crystal contexts indicate that the RNAP clamp can adopt different conformational states, ranging from an open state to a closed state (Fig. 1A; 1-9). The open and closed states differ by a ≥20° swinging motion of the clamp about a hinge region, referred to as the "switch region," located at the base of the clamp, and by a ≥20 Å displacement of residues at the tip of the clamp. It has been hypothesized that the RNAP clamp adopts different conformational states not only in crystals, but also in solution and that clamp conformational dynamics is important for function.

*Corresponding author Phone: 732-445-5179 (RHE) Fax: 732-445-5735 (RHE) ebright@waksman.rutgers.edu.

Supplementary Materials
www.sciencemag.org

In this work, we used single-molecule fluorescence resonance energy transfer (smFRET; 10-15) to measure bacterial RNAP clamp conformation in solution at each step in transcription initiation and elongation. We monitored distances between a fluorescent probe, serving as donor, incorporated at the tip of the clamp and a fluorescent probe, serving as acceptor, incorporated at the tip of the β pincer (Fig. 1A).

To incorporate probes site-specifically, we used a procedure comprising unnatural amino acid mutagenesis (16), Staudinger ligation (17,18), and RNAP reconstitution (Figs. 1B, S1-S3) (19). The procedure involved: (i) preparation of β' and β subunits containing 4-azidophenylalanine at the sites of interest (accomplished by expressing engineered genes containing nonsense codons at sites of interest using cells that contained an engineered suppressor-tRNA/aminoacyl-tRNA-synthase pair in media that contained 4-azidophenylalanine; Fig. S2A); (ii) incorporation of the fluorescent probes Cy3B (donor) and Alexa647 (acceptor) by azide-specific chemical modification (accomplished by Staudinger ligation using phosphine derivatives of fluorescent probes; Figs. S2B,C); and (iii) in vitro reconstitution of RNAP core ($\beta'\beta\alpha^{I}\alpha^{II}\omega$) or RNAP holoenzyme (RNAP core plus specificity factor σ).

To monitor distances between fluorescent probes, we used confocal optical microscopy with alternating laser excitation (ALEX; 11-15) to quantify smFRET in single molecules of RNAP freely diffusing in solution (Figs. S4-S5). ALEX allows filtering of data to consider only molecules that contain both the donor and the acceptor, eliminating complications due to incompletely labelled and incompletely assembled complexes (11-15). The results provide equilibrium population distributions of donor-acceptor smFRET efficiencies, E, and enable the calculation of donor-acceptor distances, R (11-15).

To relate smFRET results to RNAP clamp conformations, we compared observed smFRET efficiencies, E, to calculated smFRET efficiencies, E_{calc}, for each of a set of 18 structural models with RNAP clamp conformations ranging from fully open to fully closed in 2° increments (Figs. 1C, S6-S7).

Transcription initiation and transcription elongation are multistep reactions (20): (i) RNAP binds to promoter DNA, yielding an RNAP-promoter closed complex, in which DNA is double-stranded and is not yet loaded into the RNAP active-center cleft (RPc; where "closed" refers to the fact the DNA is dsDNA); (ii) RNAP loads DNA into, and unwinds DNA in, the RNAP active-center cleft, yielding an RNAP-promoter open complex (RPo; where "open" refers to the fact the DNA is partly ssDNA); (iii) RNAP synthesizes the first ~10 nt of RNA using a "scrunching" mechanism, in which RNAP remains stationary on promoter DNA and pulls downstream DNA into itself (14,21), as an RNAP-promoter initial transcribing complex (RPitc); and (iv) RNAP escapes the promoter and synthesizes the rest of the RNA using a "stepping" mechanism, in which RNAP translocates relative to DNA (22), as a transcription elongation complex (RDe).

In a first set of experiments, we examined RNAP clamp conformation in free RNAP holoenzyme containing the principle σ factor, σ^{70}, and in free RNAP core. We observed that RNAP-σ^{70} holoenzyme exhibited a broad, multimodal distribution of smFRET efficiencies (Fig. 2A, first panel). The distribution could be fitted with three Gaussians, corresponding to three subpopulations: (i) a major subpopulation with mean $E = 0.15$ and mean $R = 81$ Å, corresponding to an open clamp state; (ii) a minor subpopulation with mean $E = 0.28$ and mean $R = 69$ Å corresponding to a closed clamp state in which the clamp is rotated inward by ~14°; and (iii) a minor subpopulation with mean $E = 0.40$ and mean $R = 64$ Å, corresponding to one or more "collapsed" clamp state, more closed than any RNAP crystal structure to date, in which the clamp is rotated inward by ~22° (Fig. 1C, red boxes; Fig. 2A,

first panel; Table S1). The observed open, closed, and collapsed clamp states have RNAP active-center-cleft solvent-accessible widths of, respectively, ~20 Å (sufficient to accommodate dsDNA), ~12 Å (sufficient to accommodate ssDNA, but insufficient to accommodate dsDNA), and ~8 Å (insufficient to accommodate either dsDNA or ssDNA). We conclude that the RNAP clamp can adopt open, closed, and collapsed states in solution. We further conclude that the open state, the dimensions of which allow loading of dsDNA into the active-center cleft, is the predominant state in free RNAP-σ^{70} holoenzyme in solution.

Identical results were obtained with RNAP core (Fig. 2D). We conclude that clamp conformational dynamics are an intrinsic property of RNAP core and are not dependent on association of RNAP core with σ^{70}.

In the next set of experiments, we examined RNAP clamp conformation at each step in σ^{70}-dependent transcription initiation and in transcription elongation. We started with a sample of RNAP-σ^{70} holoenzyme (Fig. 2A, first panel). Upon the addition of DNA and formation of RPo (Fig. S1A), the distribution of smFRET efficiencies became narrow and unimodal, and only a subpopulation corresponding to a closed clamp state, with the clamp rotated inward by ~16°, was observed (Figs. 2A and S7-S10, second panels). We conclude that, after the loading of DNA into, and unwinding of DNA in, the RNAP active-center cleft to form RPo, the RNAP clamp is closed. We speculate that direct interactions between negatively charged DNA in the active-center cleft and the positively charged inner face of the clamp trigger clamp closure.

Upon the further addition of an NTP subset yielding RPitc (Fig S1A), no further change in the distribution of smFRET efficiencies was observed; only the subpopulation corresponding to a closed clamp state, with the clamp rotated inward by ~16°, was observed (Fig. 2A, third panel). Equivalent results were obtained for RPitc containing 2, 4, or 7 nt of RNA (Figs. S8-S9). We conclude that, upon the transition to RPitc--despite the synthesis of up to 7 nt of RNA through a scrunching mechanism that entails the unwinding and repositioning of up to 5 bp of DNA (14,20)--no change in clamp conformation occurs.

Upon the further addition of an NTP subset yielding RDe (Fig. S1A), no further change in distribution was observed; only a subpopulation corresponding to the closed clamp state, with the clamp rotated by ~16°, was observed (Figs. 2A, fourth panel). Equivalent results were obtained with RDe containing a 14 nt RNA product (which does not extend beyond the RNAP RNA exit channel) and RDe containing a 15 nt RNA product (which extends beyond the RNAP RNA exit channel) (Figs. S8-S9), and with RDe containing σ^{70} and not containing σ^{70} (Figs. S8-S9; 13). We conclude that, upon the transition to RDe--despite transition to a stepping mechanism of RNA synthesis (22), filling of the RNA exit channel, and optional release of σ^{70} (13)--no change in clamp conformation occurs.

Control experiments validate these observations. To rule out complications from complexes lacking σ^{70}, we performed three-color ALEX experiments (15) analyzing complexes containing a third fluorescent probe, Alexa488, on σ^{70} and considering only molecules that contained all three fluorescent probes (Fig. 2B). To rule out complications from complexes lacking DNA, we performed analogous three-color ALEX experiments, analyzing complexes containing a third fluorescent probe, Alexa488, on DNA (Fig. 2C). To rule out complications due to RNAP-probe interactions, we performed experiments using reversed donor and acceptor probe sites, different probe sites, and/or different donors and acceptors (Fig. S10 and data not shown).

In a next set of experiments, to assess RNAP clamp conformation in intermediates in formation of RPo, we analyzed transcription initiation by RNAP holoenzyme containing the

alternate σ factor σ^{54} (Fig 3). In contrast to RNAP-σ^{70} holoenzyme, which forms unstable RPc (20), RNAP-σ^{54} holoenzyme forms a stable RPc and undergoes isomerization from RPc to RPo only upon the binding of an AAA+ ATPase, such as NtrC1, and ATP hydrolysis (Fig. 3A; 23). This enables trapping and analysis of RPc and of intermediates in the isomerization of RPc to RPo (Figs. 3A,S11; 23). We analyzed clamp conformation in RNAP-σ^{54} holoenzyme, RPc (formed by adding DNA to RNAP-σ^{54} holoenzyme), RPc +NtrC1 (formed by adding NtrC1 to RPc), RPi1 (formed by adding the ground-state ATP analog ADP-BeF_x to RPc+NtrC1), RPi2 (formed by adding the transition-state ATP analog ADP-AlF_x to RPc+NtrC1) and RPo (formed by adding ATP to RPc+NtrC1) (Fig. 3A). RNAP-σ^{54} holoenzyme exhibited the same distribution of clamp states as RNAP-σ^{70} holoenzyme: a major subpopulation with an open clamp, a minor subpopulation with a closed clamp (clamp rotated inward by ~14°), and a minor subpopulation with a collapsed clamp (clamp rotated inward by ~24°)--consistent with the conclusion that clamp conformation in free RNAP is an intrinsic property of RNAP core (Fig. 3B, first panel). Upon the formation of RPc, RPc+NtrC1, RPi1, and RPi2, the open clamp state continued to predominate, the closed clamp state continued to be observed as a minor subpopulation, and the collapsed state disappeared (Fig 3B, second through fifth panels). Upon the formation of RPo, the distribution narrowed, and only a closed clamp state, with the clamp rotated inward by ~12°, was observed (Fig 3B, sixth subpanel). We conclude that the RNAP clamp predominantly is open in RPc and in all intermediates on the pathway of isomerization of RPc to RPo, and closes only upon loading of DNA into, and unwinding of DNA in, the RNAP active-center cleft to form RPo. These results support the conclusion that direct interactions between loaded, unwound DNA and the clamp trigger clamp closure.

The antibiotics myxopyronin (Myx), corallopyronin (Cor), and ripostatin (Rip) inhibit the isomerization of RPc to RPo through interactions with the RNAP switch region, the hinge that mediates opening and closing of the RNAP clamp (24-26). Bacteriophage T7 Gp2 inhibits the isomerization of RPc to RPo through interactions with a site within the RNAP active-center cleft, on or near the inner face of the clamp (27,28). It has been hypothesized that these inhibitors function by preventing clamp opening and thereby preventing loading of DNA into, and unwinding of DNA in, the active-center cleft ("hinge jamming" hypothesis; 24,26-28). We assessed effects of these inhibitors on RNAP clamp conformation in RNAP-σ^{70} holoenzyme in solution. We find that all four inhibitors depopulate the open clamp state, leaving only closed and collapsed clamp states (states in which the clamp is rotated inward by ~8° to ~26°; Fig. 4A,C). Analogous experiments assessing effects of one of the four inhibitors, Myx, on σ^{54}-dependent transcription initiation show that Myx also depopulates the open state in RNAP-σ^{54} holoenzyme and in RPc (Figs. 4C, S12). In contrast, the inhibitors rifampin (Rif), streptolydigin (Stl), and CBR703 (CBR), which inhibit steps in transcription subsequent to isomerization of RPc to RPo (29), do not affect clamp conformation (Figs. 4B,C). A Gp2 mutant defective in binding to RNAP (27) does not affect clamp conformation (Fig. S13). We propose, consistent with the hinge-jamming hypothesis, that Myx, Cor, Rip, and Gp2 prevent clamp opening and inhibit the isomerization of RPc to RPo by preventing loading of DNA into, and unwinding of DNA in, the RNAP active-center cleft (Fig. 4C).

We infer that the RNAP clamp is predominantly, and likely obligatorily, open in free RNAP and RPc, but is closed--rotated inward by ~12 to ~16°--in RPo, RPitc, and RDe. We propose that clamp opening enables the loading of DNA into, and the unwinding of DNA in, the RNAP active-center cleft during the isomerization of RPc to RPo. We propose that clamp closure is induced or stabilized by direct interactions between DNA inside the active-center cleft and the clamp, and that clamp closure is responsible for the high stability of RPo and the high stability and processivity of RDe.

We speculate that the clamp may reopen in subsequent steps in the transcription cycle that are marked by low stability and low processivity, including transcription pausing and transcription termination. Consistent with this hypothesis, a crystal structure of RDe containing an RNA hairpin associated with pausing and termination shows an open clamp (7). Further consistent with this hypothesis, the transcription factors NusG and Spt4/5, which inhibit pausing and termination, bridge the clamp and the opposite RNAP pincer, in a manner likely to inhibit clamp opening (30).

Supplementary Material

Refer to Web version on PubMed Central for supplementary material.

Abbreviations

RNAP	RNA polymerase
RP_o	RNAP-promoter open complex
RP_{itc}	RNAP-promoter initial transcribing complex
RD_e	RNAP-DNA elongation complex
NTP	nucleoside triphosphate
FRET	fluorescence resonance energy transfer
ALEX	alternating-laser excitation

REFERENCES

1. Zhang G, et al. Crystal structure of *Thermus aquaticus* core RNA polymerase at 3.3 Å resolution. Cell. 1999; 98:811. [PubMed: 10499798]
2. Cramer P, Bushnell D, Kornberg R. RNA polymerase II at 2.8Å resolution. Science. 2001; 292:1863. [PubMed: 11313498]
3. Gnatt A, Cramer P, Fu J, Bushnell D, Kornberg R. RNA polymerase II elongation complex at 3.3 Å resolution. Science. 2001; 292:1876. [PubMed: 11313499]
4. Murakami K, Masuda S, Darst S. RNA polymerase holoenzyme at 4 Å resolution. Science. 2002; 296:1280. [PubMed: 12016306]
5. Vassylyev D, et al. Crystal structure of a bacterial RNA polymerase holoenzyme at 2.6 Å resolution. Nature. 2002; 417:712. [PubMed: 12000971]
6. Vassylyev D, Vassylyeva M, Perederina A, Tahirov T, Artsimovitch I. Structural basis for transcription elongation by bacterial RNA polymerase. Nature. 2007; 448:157. [PubMed: 17581590]
7. Tagami S, et al. Crystal structure of bacterial RNA polymerase bound with a transcription inhibitor protein. Nature. 2010; 468:978. [PubMed: 21124318]
8. Landick R. RNA polymerase clamps down. Cell. 2001; 105:567. [PubMed: 11389826]
9. Darst S, et al. Conformational flexibility of bacterial RNA polymerase. Proc. Natl. Acad. Sci. USA. 2002; 99:4296. [PubMed: 11904365]
10. Materials and methods are available as supporting material on *Science* Online.
11. Kapanidis A, et al. Analysis of structure and interactions by alternating-laser excitation of single molecules. Proc. Natl. Acad. Sci. USA. 2004; 101:8936. [PubMed: 15175430]
12. Lee N, et al. Accurate FRET measurements within single diffusing biomolecules using alternating-laser excitation. Biophys. J. 2005; 88:2939. [PubMed: 15653725]
13. Kapanidis A, et al. Retention of transcription initiation factor σ^{70} in transcription elongation: single-molecule analysis. Mol. Cell. 2005; 20:347. [PubMed: 16285917]

14. Kapanidis A, et al. Initial transcription by RNA polymerase proceeds through a DNA-scrunching mechanism. Science. 2006; 314:1144. [PubMed: 17110578]
15. Lee N, et al. Three-color alternating-laser excitation of single molecules. Biophys. J. 2007; 92:303. [PubMed: 17040983]
16. Chin J, et al. Addition of p-azido-L-phenylalanine to the genetic code of *Escherichia coli*. J. Amer. Chem. Soc. 2002; 124:9026. [PubMed: 12148987]
17. Saxon E, Bertozzi C. Cell surface engineering by a modified Staudinger reaction. Science. 2000; 287:2007. [PubMed: 10720325]
18. Chakraborty A, Wang D, Ebright Y, Ebright R. Azide-specific labeling of biomolecules by Staudinger-Bertozzi ligation phosphine derivatives of fluorescent probes suitable for single-molecule fluorescence spectroscopy. Meths. Enzymol. 2010; 472:19.
19. Tang H, Severinov K, Goldfarb A, Ebright R. Rapid RNA polymerase genetics. Proc. Natl. Acad. Sci. USA. 1995; 92:4902. [PubMed: 7761421]
20. Saecker R, Record MT, Dehaseth P. Mechanism of bacterial transcription initiation. J. Mol. Biol. 2011; 412:754. [PubMed: 21371479]
21. Revyakin A, Liu C, Ebright RH, Strick T. Abortive initiation and productive initiation by RNA polymerase involve DNA scrunching. Science. 2006; 314:1139. [PubMed: 17110577]
22. Abbondanzieri E, Greenleaf W, Shaevitz J, Landick R, Block S. Direct observation of base-pair stepping by RNA polymerase. Nature. 2005; 438:460. [PubMed: 16284617]
23. Ghosh T, Bose D, Zhang X. Mechanisms for activating bacterial RNA polymerase. FEMS Microbiol. Rev. 2010; 34:611. [PubMed: 20629756]
24. Mukhopadhyay J, et al. The RNA polymerase switch region is a target for inhibitors. Cell. 2008; 135:295. [PubMed: 18957204]
25. Belogurov G, et al. Transcription inactivation through local refolding of the RNA polymerase structure. Nature. 2009; 457:332. [PubMed: 18946472]
26. Srivastava A, et al. New target for inhibition of bacterial RNA polymerase: 'switch region'. Curr. Opin. Microbiol. 2011; 14:532. [PubMed: 21862392]
27. Camara B, et al. T7 phage protein Gp2 inhibits the *Escherichia coli* RNA polymerase by antagonizing stable DNA strand separation near the transcription start site. Proc. Natl. Acad. Sci. USA. 2010; 107:2247. [PubMed: 20133868]
28. Mekler V, Minakhin L, Sheppard C, Wigneshweraraj S, Severinov K. Molecular mechanism of transcription inhibition by phage T7 gp2 protein. J. Mol. Biol. 2011; 413:1016. [PubMed: 21963987]
29. Mariani R, Maffioli S. Bacterial RNA polymerase inhibitors. Curr. Med. Chem. 2009; 16:430. [PubMed: 19199915]
30. Hartzog G, Kaplan C. Competing for the clamp. Mol. Cell. 2011; 43:161. [PubMed: 21777806]

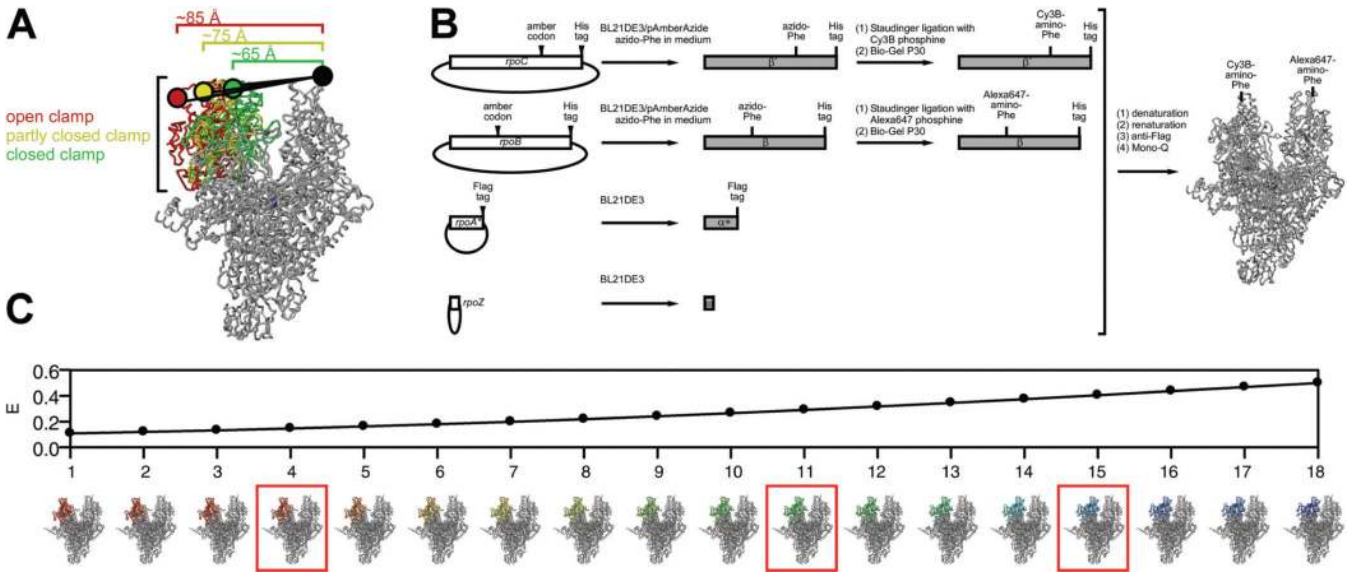

Fig. 1. Determination of RNAP clamp conformation in solution

(A) Measurement of smFRET between fluorescent probes incorporated at the tips of the RNAP β' pincer (clamp) and the RNAP β pincer. Open (red), partly closed (yellow), and closed (green) RNAP clamp conformational states are as observed in crystal structures (PDB 1I3Q, 1HQM, and 1I6H). σ and the β' non-conserved domain are omitted for clarity in this and subsequent figures.

(B) Incorporation of fluorescent probes at the tips of the RNAP β' pincer (clamp) and the RNAP β pincer, by unnatural amino acid mutagenesis to incorporate 4-azidophenylalanine at sites of interest in β' and β, followed by Staudinger ligation to incorporate fluorescent probes at 4-azidophenylalanines in β' and β, followed by in vitro reconstitution of RNAP from labelled β' and β and unlabelled α* (covalently linked α-N-terminal-domain dimer) and ω(see Supplemental Methods). Plasmids, genes, and proteins are shown as ovals, open bars, and closed bars, respectively.

(C) Relationship between smFRET efficiencies, *E*, and RNAP clamp conformational states (see Supplemental Methods). The red boxes denote the open (model 4; red), closed (model 11; green), and collapsed (model 15; blue) clamp states observed in this work for RNAP-σ^{70} holoenzyme (Fig. 2).

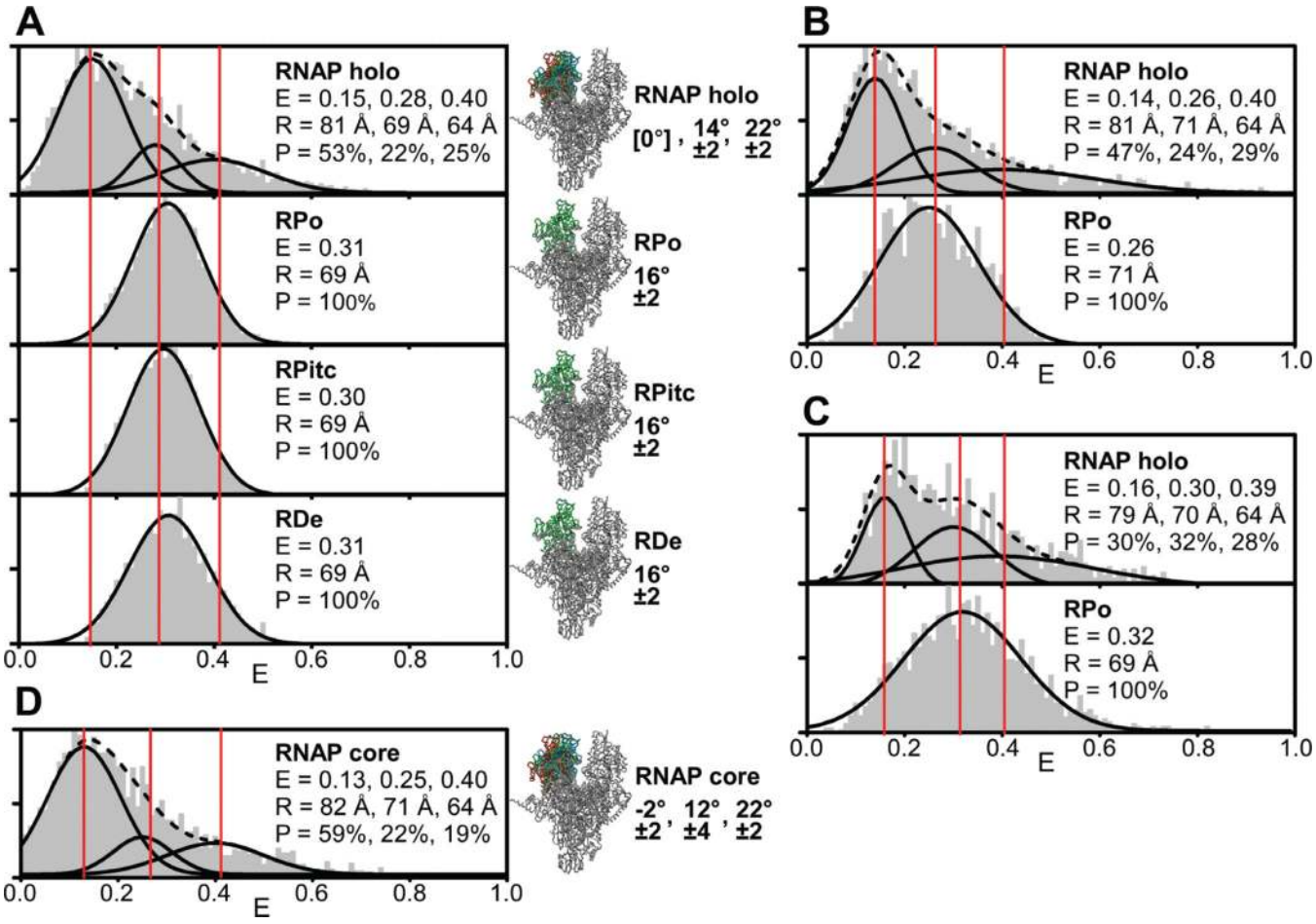

Fig. 2. RNAP clamp conformation in σ^{70}-dependent transcription initiation and elongation

Panels show histograms and Gaussian fits of observed donor-acceptor smFRET efficiencies, *E* (at left); mean *E*, mean *R*, and percentage, *P*, for each subpopulation (in inset at left); inferred structural states of the RNAP clamp (at right; colored as in Fig. 1C); and inferred extents of closure of the RNAP clamp (at far right; in degrees ±SEM relative to the open state). The vertical red lines denote mean *E* of the open, closed, and collapsed states in RNAP-σ^{70} holoenzyme.

(A) RNAP clamp conformation in RNAP holoenzyme, RPo, RPitc (4 nt RNA), and RDe (14 nt RNA).

(B) Control three-color FRET experiments with third probe on σ^{70} (data filtered to include only molecules containing σ^{70}).

(C) Control three-color FRET experiments with third probe on DNA (data for RPo filtered to include only molecules containing DNA).

(D) RNAP clamp conformation in RNAP core.

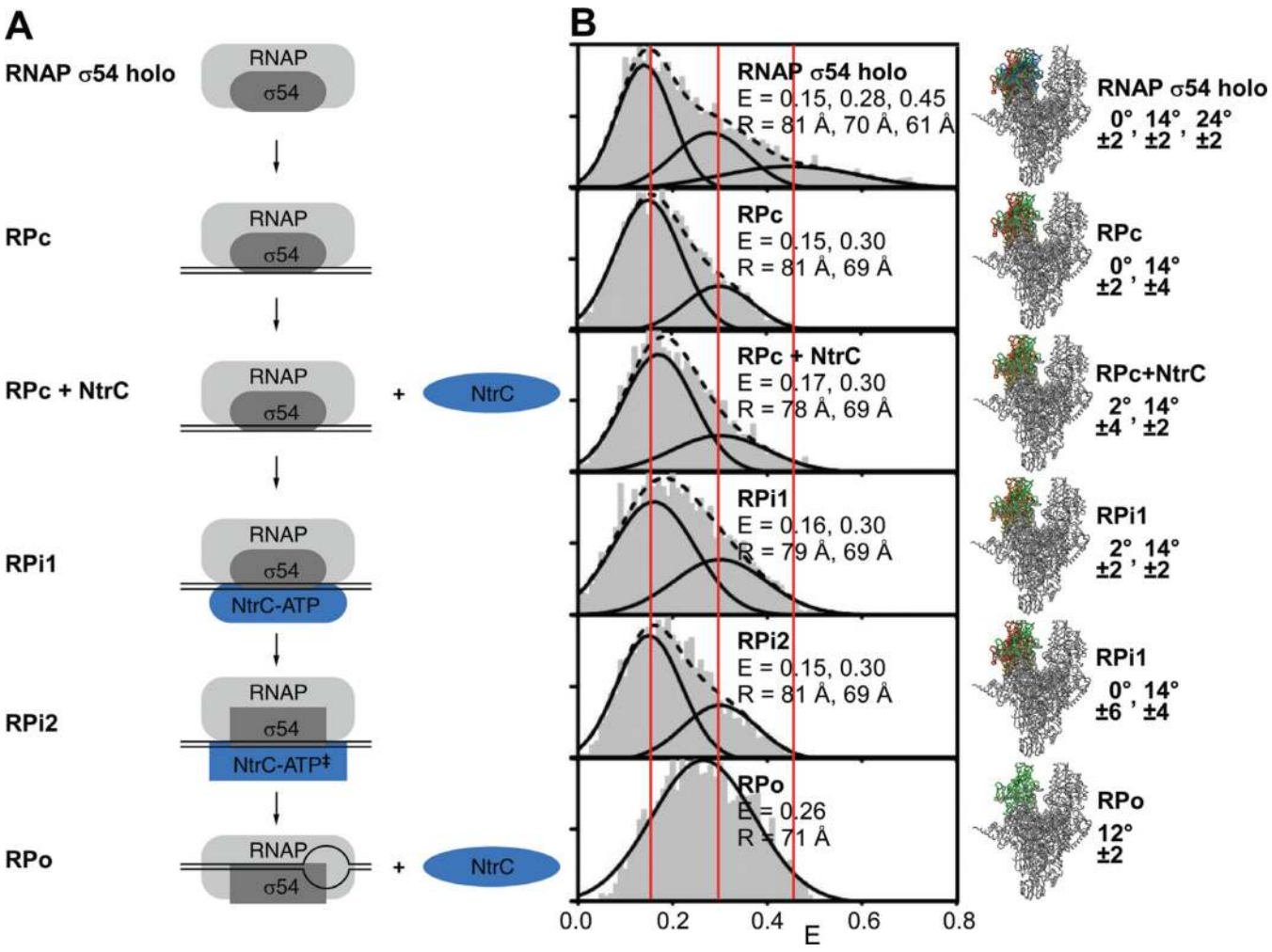

Fig. 3. RNAP clamp conformation in σ^{54}-dependent transcription initiation

(A) Intermediates in σ^{54}-dependent transcription initiation (23).

(B) RNAP clamp conformation in RNAP-σ^{54} holoenzyme, RPc, RPc+NtrC1, RPi1, RPi2, and RPo.

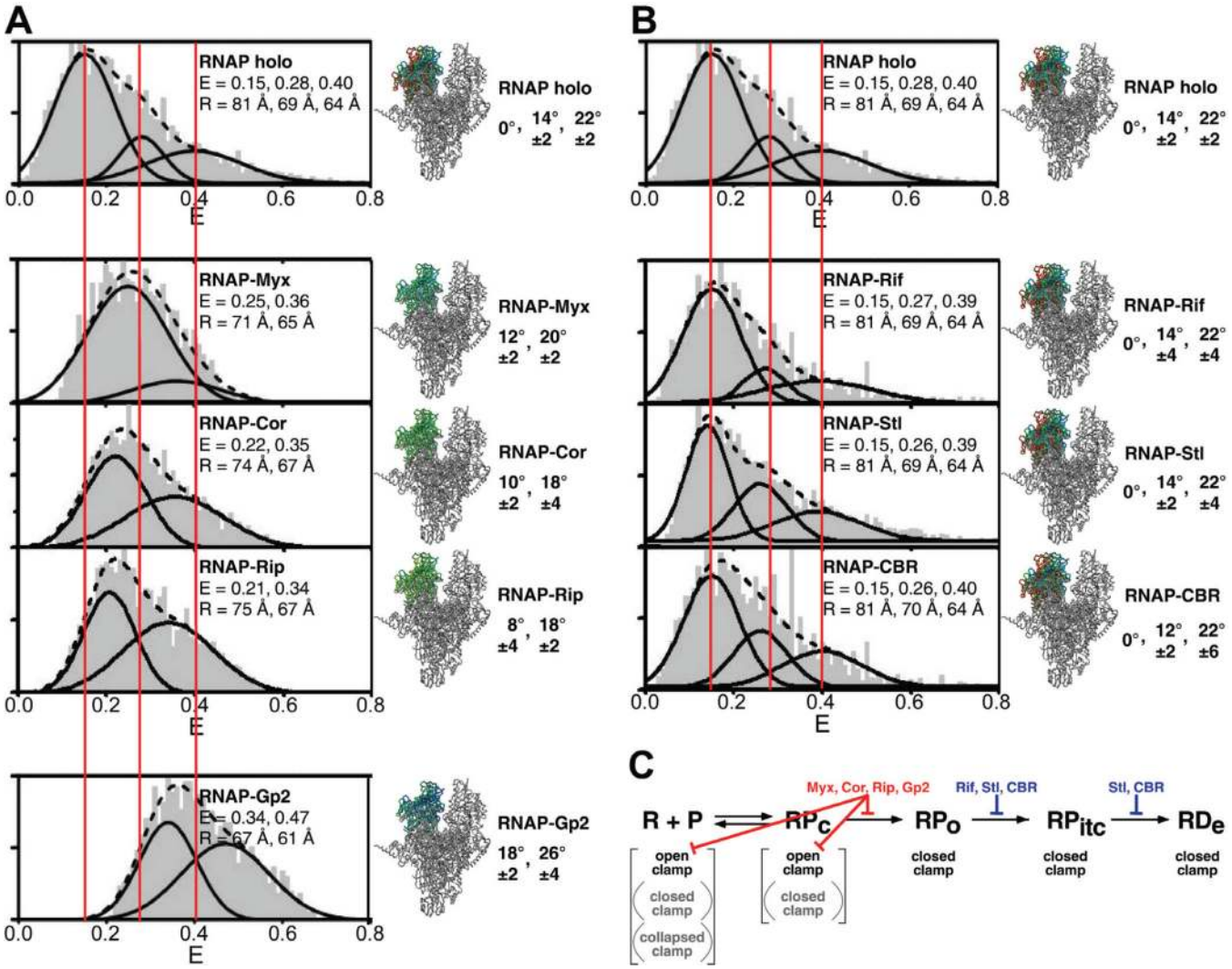

Fig. 4. Effects of inhibitors on RNAP clamp conformation

(A) Effects of inhibitors that block the isomerization of RPc to RPo: Myx, Cor, Rip, and Gp2.

(B) Effects of inhibitors that block steps subsequent to the isomerization of RPc to RPo: Rif, Stl, and CBR.

(C) Summary. The major clamp conformation at each step in transcription initiation and transcription elongation stage is shown in black. Minor clamp conformations are shown in gray. Myx, Cor, Rip, and Gp2, which inhibit the isomerization of RPc to RPo (vertical red line), inhibit clamp opening (slanted red lines); Rif, Stl, and CBR, which inhibit steps subsequent to the isomerization of RPc to RPo (vertical blue lines), do not inhibit clamp opening.